Desalination and Water Treatment
www.deswater.com

doi: 10.5004/dwt.2018.22094

117 (2018) 66–77
June

Properties and application of cellulose membranes with graphene oxide addition for removal of heavy metals from aqueous solutions

Beata Fryczkowska*, Dorota Biniaś, Czesław Ślusarczyk, Janusz Fabia, Jarosław Janicki

Faculty of Materials, Civil and Environmental Engineering, Institute of Textile Engineering and Polymer Materials, University of Bielsko-Biala, Willowa 2, 43-309 Bielsko-Biala, Poland, Tel. +49 338279114; Fax: +48 33 8279100; emails: bfryczkowska@ath.bielsko.pl (B. Fryczkowska), dbinias@ath.bielsko.pl (D. Biniaś), cslusarczyk@ath.bielsko.pl (C. Ślusarczyk), jfabia@ath.bielsko.pl (J. Fabia), jjanicki@ath.bielsko.pl (J. Janicki)

Received 7 December 2017; Accepted 20 February 2018

ABSTRACT

The paper presents results of research on the properties and application of cellulose-based (CEL) composite membranes with graphene oxide (GO) addition for the removal of heavy metals from aqueous solutions. Composite membranes (GO/CEL) were prepared by phase inversion from CEL solutions in 1-ethyl-3-methylimidazolium acetate (EMIMAc) containing addition of GO in the form of nanoparticle dispersion in N,N-dimethylformamide (DMF). The paper demonstrates how the amount of GO addition influences the structure and physicochemical and separation properties of GO/CEL composite membranes. Infrared spectroscopy, thermal analysis, X-ray crystallography and scanning electron microscopy were used in structural studies. Investigations of transport properties have shown that the introduction of 2%, 10% and 20% of GO into the composite membrane improves its transport properties, resulting in a 2-, 5- and 10-fold increase in permeate flux. The paper also investigated the use of GO/CEL composite membranes in removal of selected heavy metals (lead, zinc, cobalt and nickel) from aqueous solutions determined by atomic absorption spectrometry. It was found that ~100% removal of heavy metals is obtained for membranes containing 2%, 10% and 20% of GO in the cellulose matrix.

Keywords: Cellulose; Graphene oxide; Heavy metals; Membrane; Transport properties; Rejection

1. Introduction

Water pollution caused by toxic heavy metals (cadmium, chromium, copper, mercury, nickel, lead, zinc) discharged from industrial and agricultural sources is one of the most serious environmental and public concerns. Water contaminated with heavy metals also penetrates into soils, causing their pollution. Although many heavy metals are needed at trace element levels for humans, animals and plants, their excessive amounts can cause many toxic effects. Soil contamination can be removed by physical, chemical, biological and combined remediation methods [1]. Different physical or chemical methods can be used to remove heavy metal ions from water, including adsorption or membrane process (ultrafiltration [UF], reverse osmosis [RO], nanofiltration [NF] and electrodialysis [ED]) [2–5]. An important feature of the technique used is its effectiveness and low price.

Cellulose is one of the most widespread, inexpensive and biodegradable polymers used in the textile, chemical, pharmaceutical, construction and energy industries [6,7]. The presence of hydrogen bonds [8,9] in cellulose makes the polymer insoluble in water and in most solvents [10,11]. Thus, various systems, such as: NaOH/CS_2, N-methylmorpholine-N-oxide and water mixture (NMMO/H_2O), LiCl/dimethylacetamide (DMAc), dimethyl sulfoxide and tetrabutylammonium fluoride mixture (DMSO/TBAF) and ionic liquids are used for processing of cellulose [12]. Ionic liquids are often called "green" solvents [13], due to their biodegradability and low

* Corresponding author.

Presented at the 13th Conference on Microcontaminants in Human Environment, 4–6 December 2017, Czestochowa, Poland.

toxicity [14]. These compounds may replace traditional cellulose systems in the future [9,15,16]. The cellulose dissolved in ionic liquids can easily be precipitated using polar solvents [9]. Regenerated cellulose in the form of flocs, fibres or membranes [16–18] hydrogels and aerogels, microspheres and beads [12] is less crystalline and more porous [18–22].

An interesting and modern material used for the production of polymer composites is graphene oxide (GO). GO has many different oxygen-containing functional groups, such as epoxy, hydroxyl, carbonyl, carboxyl [23,24]. Oxygen groups give hydrophilic properties to GO, making it easy to form its stable aqueous dispersions [25,26] at concentrations above 3 mg/mL [27]. GO can also be dispersed in organic solvents such as N,N-dimethylformamide, N-methyl-2-pyrrolidone, tetrahydrofuran and ethylene glycol [28]. GO is also used in membranes, along with carbon nanotubes [29–32] and graphene [33–35]. It allows obtaining thin, monolayer films [30–33] which can be used for desalination and UF [33,34,40,41] as well as membrane distillation [42].

The diversity of oxygen functional groups arranged on the GO surface makes it easy to be dispersed in polymer with functional groups to form durable bonds [24,43]. The polymer that meets the above requirements is the cellulose from which Liu et al. [44] obtained cellulose composite membranes by filtration of GO solution on pure cellulose membrane. Other researchers mixed subhydrolized microcrystalline cellulose in the form of suspension with GO dispersion and then dried it obtaining membranes [45]. Kim et al. [46] used NMMO as a solvent for obtaining GO/cellulose composite membranes. Nanocomposite aerogels, on the other hand, were obtained from bamboo fibres dissolved in a NaOH/PEG mixture to which water dispersion of GO was added [47]. Zhang et al. [48] described the method of obtaining microbeads of cellulose with GO addition in NaOH/urea solution. GO-containing microbeads were obtained in the process of bacterial cellulose synthesis [49]. Other researchers mixed the grinded bacterial cellulose with GO dispersion and formed a composite film [50]. Rui-Hong et al. [51] obtained hydrogel by introducing NaOH and urea and cellulose into the aqueous dispersion of GO, and mixing it with PVA solution. Still other researchers [52] received composite membranes using a layer-by-layer method.

This paper presents the results of previously unreported studies on GO/CEL composite membrane formation from a homogeneous dispersion of nanosized GO additive in the cellulose solution as well as the effect of adding GO nanoparticles on the structural and morphology and transport properties of the CEL membranes. First, GO was synthesized using the modified Hummers' method [53] and then dispersed in N,N-dimethylformamide (DMF). Cellulose was dissolved in a low-temperature ionic liquid: 1-ethyl-3-methylimidazol acetate (EMIMAc) [54,55], in contrast to the work of Tang et al. [52] who used [Bmim]Cl. A method of combining the cellulose solution with the dispersion (GO) was developed to obtain a homogeneous solution from which the composite membranes were then formed, using phase inversion method, by coagulation in distilled water. The GO/CEL membranes are a composite in which cellulose chains containing hydroxyl groups form hydrogen bonds with oxygen functional groups on the surface and edges of GO flakes The interactions between cellulose and GO were previously reported by Tang et al. [52], and Wan and Li [47] (Fig. 1). This paper also presents previously unreported research on the effect of the presence of heavy metal ions on the transport properties and high degree of rejection of composite membranes GO/CEL.

2. Experimental

2.1. Materials

Cellulose (long fibres), ionic liquid (EMIMAc), graphite powder < 20 μm, were purchased from Sigma-Aldrich (Poland, Poznań). $NaNO_3$, 98% H_2SO_4, $KMnO_4$, 30% H_2O_2, DMF, NaCl, $Co(NO_3)_2$, $Ni(NO_3)_2$, $Pb(NO_3)_2$, $ZnCl_2$ were purchased from Avantor Performance Materials Poland S.A. (Poland, Gliwice). All the chemicals were used without further purification.

2.2. GO synthesis and preparation of GO/DMF dispersion

GO was obtained according to modified Hummers' method [53]. GO synthesis and its properties (X-ray diffraction [XRD], thermal analysis [DSC], infrared spectroscopy [FTIR]) as well as their results were very similar to those obtained in our earlier work [56]. Wet GO was dried in a

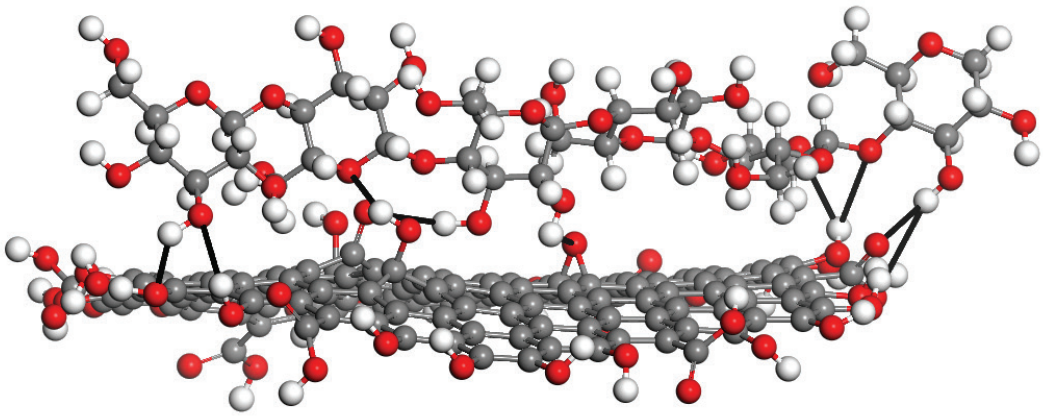

Fig. 1. Schematic diagram hydrogen bonds (black bold line) between GO (bottom) and CEL macromolecular chains (top). Grey balls – carbon, white balls – hydrogen, red balls – oxygen.

laboratory drier at 60°C to obtain a brown precipitate which was then dispersed in DMF on an ultrasonic bath to obtain a 5.2% GO/DMF dispersion.

2.3. Membrane formation

Initially, a 5% solution of cellulose in the EMIMAc was prepared. The mixture of cellulose and EMIMAc was thoroughly mixed and then heated in a microwave oven in intervals of 3 x 5 s, taking care that the temperature of the mixture did not exceed approximately 40°C. The resulting cellulose solutions were left for 24 h to deaerate. In order to prepare solutions for forming GO/CEL composite membranes, adequate amounts of cellulose and ionic liquid were first weighed (Table 1) and cellulose solutions were prepared as described above. Appropriate amounts of 5.2% GO/DMF solution (Table 1) were then added to the cellulose solutions, thoroughly mixed and sonicated for 15 min. The obtained GO/CEL solutions were allowed to deaerate for 24 h.

Cellulose membranes were prepared using phase inversion method. For this purpose, pre-prepared solutions were poured on a level, clean glass plate. Then a polymeric film was formed using casting knife with an adjustable thickness fixed at 0.2 mm. Finally, it was rapidly coagulated in distilled water at room temperature until the membrane was detached from the glass. A thin layer of polyester fabric followed by layers of tissue paper is used to separate the cellulose membranes. This prevents the cellulose from sticking to the filter paper and facilitates the drying of the cellulose. Membranes were dried under glass plate load.

2.4. Measurements of water flux

The transport properties of the formed membranes were tested using a Millipore Amicon 8400 UF cell with a 350 mL capacity and a 7.6 cm membrane diameter that was equipped with an equalizing tank with an 800 mL capacity. First, dry membranes were immersed in distilled water for 1 h. Then, they were treated with distilled water for an additional 2 h under a pressure of 0.2 MPa to improve the membrane stability. UF tests were performed at operational pressures of 0.1, 0.15 or 0.2 MPa. Permeate flux (J_v) was calculated using the following formula:

$$J_v = \frac{Q}{At} \tag{1}$$

where J_v is water flux (L/m^2 × h), Q is the permeate volume (L), A is the effective membrane area (m^2) and t is the permeation time (h).

2.5. Measurements of rejection

Standard solutions of $Pb(NO_3)_2$ with a concentration of 60 mg/L and NaCl, $Co(NO_3)_2$, $Ni(NO_3)_2$ and $ZnCl_2$ with concentrations of 6 mg/L were prepared to study the separation properties of the produced composite membranes. In addition, a mixture of synthetic wastewater containing 6 mg/L NaCl, $Co(NO_3)_2$, $Ni(NO_3)_2$, $ZnCl_2$ and 60 mg/L $Pb(NO_3)_2$ were prepared.

Then, 200 mL of successive standard solutions were added to the UF cell with the test membrane and the stirrer. The permeation process was carried out at a working pressure of 0.2 MPa and 20 mL doses of permeate were tapped, measuring simultaneously the time of the permeate discharge from the test tank. Permeate flux (J_v) was calculated using Eq. (1), assuming that in this case Q is the permeate volume (specific test solution).

Ion concentrations of the subsequent metals were determined using atomic absorption spectrometry (AAnalist 100 AAS, Perkin-Elmer International Rotkreuz Branch P.O., Switzerland, Rotkreuz), and the rejection coefficient (R) was calculated using Eq. (2):

$$R = \left(1 - \frac{C_p}{C_f}\right)100\% \tag{2}$$

where R is the rejection performance of the membrane (%), and C_p and C_f are the concentrations of metal ions in the permeate and feed solution (mg/L), respectively.

2.6. Analytical methods

All measurements were performed using a Nicolet 6700 FT-IR spectrometer (Thermo Electron Corp., Madison, WI, USA) equipped with photoacoustics MTEC model 300 accessory. Samples for photoacoustic testing were placed in a special snap holder. The following measurement parameters were used: resolution, 4 cm^{-1}; spectral range, 500–4,000 cm^{-1}; detector – deuterated thioglycine (DTGS); number of scans, 64. Data collection and post-processing were performed using OMNIC software (v. 8.0, Thermo Electron Corp.).

XRD investigations were performed with a URD 63 Seifert diffractometer. Cu Ka radiation was used at 40 kV and 30 mA. Monochromatization of the beam was obtained by means of a nickel filter and a pulse-height analyser. A scintillation counter was used as a detector. Diffractograms were recorded from 18° to 26° with a step of 0.01°. Each diffraction curve was corrected for polarization, the Lorentz factor and incoherent scattering.

Table 1
Composition of the solutions for the preparation of membranes

Membrane designation	"0"	A	B	C	D	E	F
Amount of 5.2% GO/DMF solution (g)	0	0.05	0.1	0.5	0.97	4.8	9.7
Amount of CEL (g)	2.5	2.5	2.5	2.5	2.5	2.5	2.5
Amount of EMIMAC (g)	47.5	47.45	47.4	47.0	46.53	42.7	37.8
Concentration of GO (% w/w)	0	0.1	0.2	1	2	10	20
Concentration of CEL (% w/w)	100	99.9	99.8	99	98	90	80

Thermal studies of the membranes were conducted using a MDSC 2920 differential scanning calorimeter (TA Instruments, Poland, Warszawa). The DSC curves obtained were analysed using the TA Instruments Universal V4.5 software package. Measurements were performed under a nitrogen atmosphere (flow rate 40 mL/min) while heating at 20°C/min from –20°C to 300°C.

Membrane surface morphologies and their cross sections were observed using a JSM 5500 LV scanning electron microscope (JEOL, Poland, Warszawa). All samples were coated with a layer of gold in a JEOL JFC 1200 vacuum coater at 3×10^{-5} torr.

3. Results and discussion

As a result of the experiment cellulose membranes ("0") and cellulose composite membranes (A–F) which differed in colour depending on the amount of GO addition were obtained (Fig. 2). In order to make images, translucent membranes were placed on filter paper. The "0" membranes are colourless, while the other diaphragms are in shades of grey. The more GO addition in the membrane, the darker composite GO/CEL membrane is.

3.1. Characterization techniques

3.1.1. Scanning electron microscopy analysis

Scanning electron microscopy (SEM) enabled the observation of the surface morphology of skin layer, the support layer and cross sections of the obtained membranes (Fig. 3). In SEM images of cross sections of membranes (Fig. 3-1), the pure cellulose membrane ("0") is observed to be compact but slightly rough, which makes it clearly distinguishable from the GO/CEL composite membranes. The cross section of membrane A and B is similar to each other. In the case of composite membranes A and B, apart from the roughness, horizontal cracks appear. In addition, 0.1% and 0.2% GO addition increases the thickness of the membranes (Figs. 3(A-1) and (B-1)). The structure of cross section C and D membranes were different from all others. Membranes containing 1% and 2% GO have a compact structure, but with visible horizontal cracks (Figs. 3(C-1) and (D-1)). By comparing the thickness of the membranes with one another, it can be seen that a 1% addition of GO to the composite membrane C reduces its thickness, which is comparable with the thickness of the "0" membrane. In SEM images of membrane E, a large numbers of horizontal cracks can be observed. The structure of membrane F cross section is very rich and diametrically different from the other ones. In Fig. 3(F-1), membrane can be observed as entirely composed of transversely arranged flakes. On the basis of microscopic observations of cross sections of the membranes, the effect of GO addition on the cellulose matrix can be easily observed. The effect of increasing the amount of GO in the composite membrane is the appearance of an increasing number of cracks, which may result from the arranging of components in the composite.

In the images (Fig. 3-2), the morphology of the skin layer of the membranes can be observed. Membrane "0" is characterized by an even, smooth surface. While the surfaces of composite membranes with small amounts of GO addition (membrane A, B, C) is very rich: it has corrugations, spherical beads and recesses. In contrast, the skin layers of membrane D, E and F are different from the others. On the relatively flat surface of these membranes, cracks and recesses are observed, the number and size of which increases with the amount of GO addition in the direction of membrane D to F.

The surface of the support layers of all membranes (Fig. 3-3) is richer in various morphological structure elements compared with the skin layer. Hollows and spherical beads, the number and size of which increase with the amount of GO addition, can be observed. In the case of membranes E and F, apart from hollows, numerous cracks appear on the surface of the support layer.

3.1.2. FTIR analysis

The molecular structure of the skin surface was investigated using the FTIR spectroscopy (Fig. 4). The characteristic wide band of the elastic O–H vibrations indicating for the formation of hydrogen bonds is observed between 3,700 and 2,400 cm^{-1} (Fig. 4(a)). We can observe the widening of this band with the quantity of GO introduced to the cellulose membranes. The GO addition probably causes loosening of the structure between of cellulose macromolecule chains and introduces additional hydroxyl groups. The band at a wavelength of approximately 2,900 cm^{-1} is the effect of the stretching vibrations of the C–H oscillator. No significant differences in this range of wave numbers indicate that the configuration of the groups containing this oscillator is preserved. There are no significant differences in the molecular structure of the system [44]. The band with a peak at approximately 1,110 cm^{-1} is the effect of oscillation of etheric C–O–C groups between the rings and the band with a peak at approximately 1,050 cm^{-1} is the result of C–O–C vibrations in the pyranose ring [44]. In the case of GO/CEL composite membranes (membranes B–F), widening of the bands from the

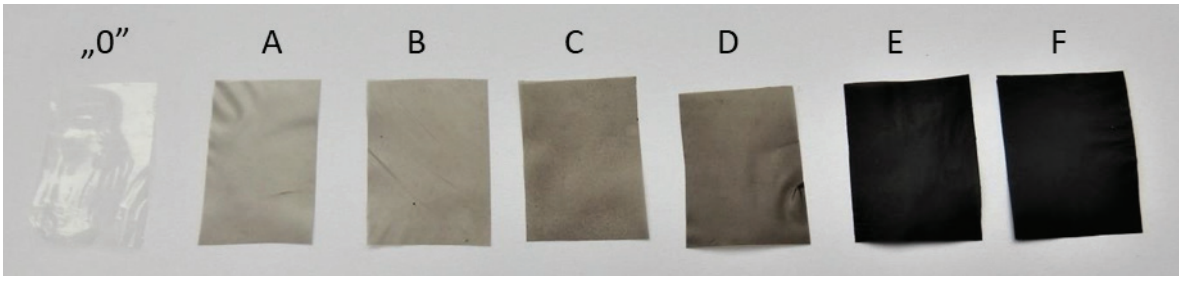

Fig. 2. Images of pure cellulose membranes ("0") and GO/CEL composite membranes (A – 0.1% GO; B – 0.2% GO; C – 1% GO, D – 2% GO; E – 10% GO; F – 2% GO, respectively).

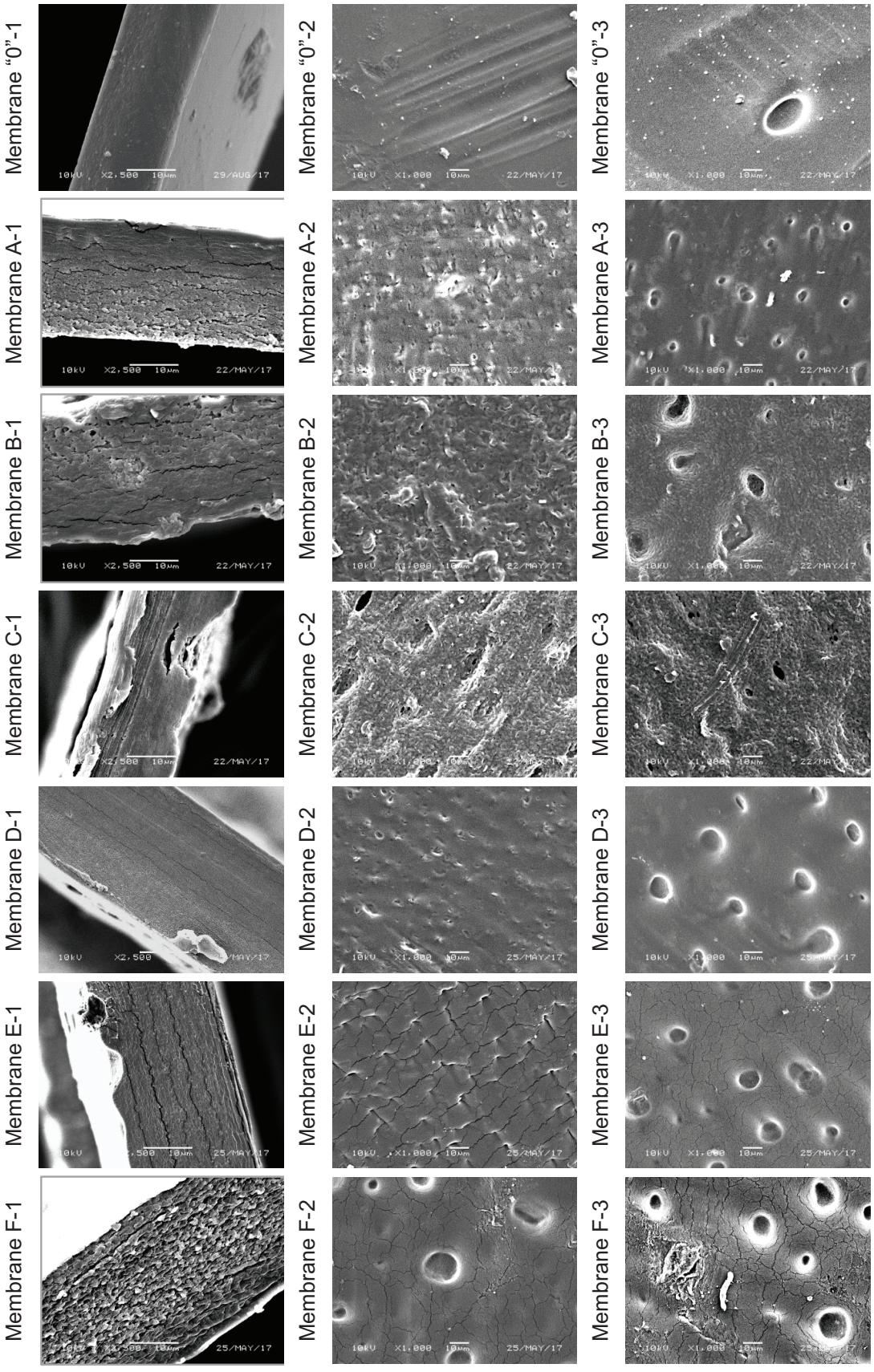

Fig. 3. SEM images for membranes: 1 – cross section; 2 – skin layer; 3 – bottom layer.

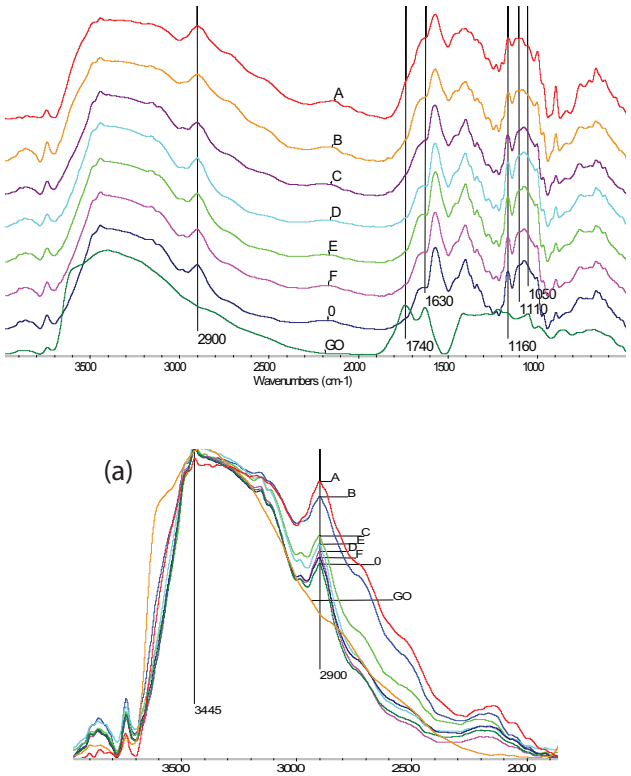

Fig. 4. FTIR spectra of pure cellulose membrane "0," GO and GO/CEL composite membranes (A–F). (a) The characteristic wide band (3,700 ÷ 2,400 cm^{-1}) of the elastic O–H indicating the formation of hydrogen bonds between GO and CEL.

wavelength of approximately 1,400 to 1,000 cm^{-1} is observed, resulting from the presence of GO in the mixture [47]. The intensity of this band slightly increases as the GO concentration in the cellulose matrix increases. For GO/CEL composite membranes, band intensities are observed at wavelengths of approximately 1,740 and 1,630 cm^{-1} corresponding to the vibration of C=O groups in GO along with the amount of GO introduced to the cellulose membranes.

3.1.3. XRD analysis

Fig. 5 shows wide angle x-ray scattering (WAXS) diffraction curves of membrane "0" (the pure cellulose) and the pure GO. The curve of cellulose exhibits the typical diffraction patterns of cellulose II crystalline structure revealed by the characteristic peak at 2θ = 12.6° and close to each two adjacent peaks at 2θ = 20.3° and 21.2°. These peaks can be indexed as (–110), (110) and (–121), respectively. The WAXS curve of the GO shows the sharp diffraction peak at 2θ = 9.0° (d-spacing = 0.98 nm) which reflects the gallery gap of the layered structure of the GO. Fig. 6 presents WAXS diffraction patterns of GO–cellulose membranes. The curves exhibit all peaks characteristic for cellulose II crystal as well as the GO peak, whose angular position is shifted towards the lower diffraction angles with the decreasing GO content. Such peak shift indicates an increase in the distance between the carbon layers in the GO. Compared with pure GO, this distance increases from 0.98 to 1.6 nm for membranes B and

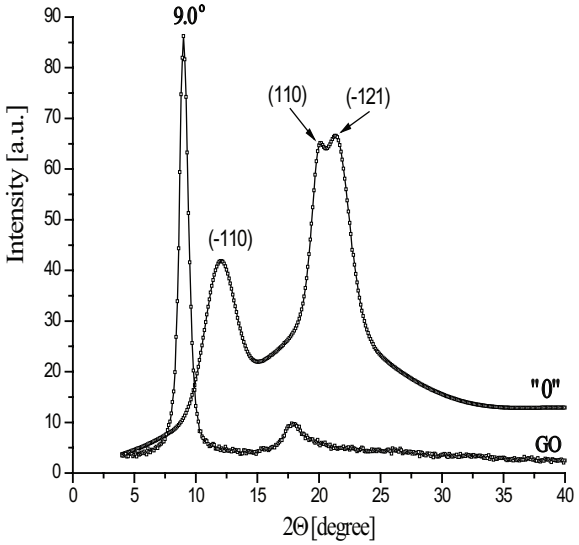

Fig. 5. WAXS patterns of membrane "0" (the pure cellulose) and the pure GO.

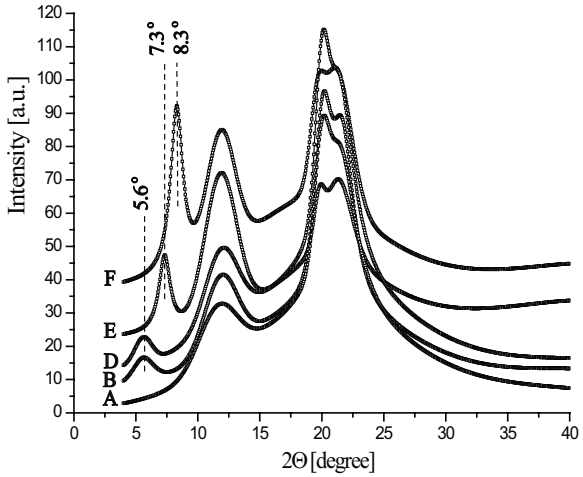

Fig. 6. Examples of WAXS patterns of cellulose membranes (the letters on the left indicate the membrane code).

D. The step-wise increase of d-spacing might be due to the interactions between the GO and cellulose by hydrogen bonds (Fig. 1), which might already be saturated at low loading of the GO. Therefore, the increase in the distance between carbon galleries in GO is more pronounced when the ratio of cellulose content to GO content increases.

3.1.4. DSC analysis

In the analysis of DSC curves, we can observe the sequence of thermal effects corresponding to the changes taking place in the material of the studied GO/CEL composite membranes during heating. In the order of rising temperature, we record successively: moisture evaporation, then GO phase decomposition and characteristic endothermic thermal effect occurring in a temperature range of 250°C–300°C, indicating the

presence of residual amounts of ionic liquid in the membrane structure, used for plastification of cellulose (Fig. 7). The first two effects are confirmed multiple times in the form of published thermogravimetric analysis (TGA) results [47,48]. The third of the observed effects was related to the presence of the ionic liquid, for which in DSC studies, in the same temperature range, a very strong endothermic peak with an enthalpy value of almost 490 J/g is observed. In case of GO/CEL composite membranes, the minimum temperature values of the discussed peak change, without specific trend against the content of GO in the samples, at a relatively narrow range of 275°C–279°C, and the corresponding enthalpy values between 68 and 74 J/g which corresponds to the 14%–15% content of ionic liquid. Although within the analysed temperature range 250°C–300°C one should be aware of the possibility of exothermic effects related to the decomposition of the cellulose matrix; however, due to the specific interaction between GO and cellulose, demonstrated inter alia in a study by Zhang et al. [48], the thermostability of the GO/CEL membrane matrix has been effectively raised to over 300°C in our case.

The characteristics of DSC curves registered for the tested membranes (Fig. 8) enable distinguishing two basic types among them: composite membranes with relatively low GO content of a few percent (B–D) and those with GO content exceeding a dozen percent (E and F).

In terms of the water evaporation effect in the samples, the corresponding minimum temperature of the $T_{w\,ev}$ endotherm and the specific enthalpy values of the $\Delta H_{w\,ev}$ transition decrease monotonically with the increase in the GO content, with slight changes within the first group of membranes (B–D) and clear, step-wise changes between groups (Table 2). The nature of the changes of the indicated parameters confirms the results obtained by SEM (Fig. 3). The diameters of pore present in the structure of composite membranes, shown in the SEM images, increase as a function of the GO modifier, which corresponds to the possibility of easier water release (moving $T_{w\,ev}$ towards increasingly lower temperatures).

Another transition that needs to be taken into account when analysing the DSC curves is the thermal dissociation of GO. This transformation is reflected in curves in the form of a characteristic endothermic effect, occurring in the temperature range of 150°C–250°C. For membranes with GO content not exceeding 2%, the discussed transition corresponds to the wide exothermic peak temperature with a maximum at $T_{GO\,d}$, oscillating in the narrow range of 218.5°C–219.6°C and the enthalpy values of $\Delta H_{GO\,d}$ slightly increasing as a function of GO content. For membranes E and F, the distribution of GO on DSC curves is different, taking the form of two non-separated exothermic peaks. One peak is placed in similar area as the one observed for membranes B–D. Second, additional peak has a maximum temperature of less

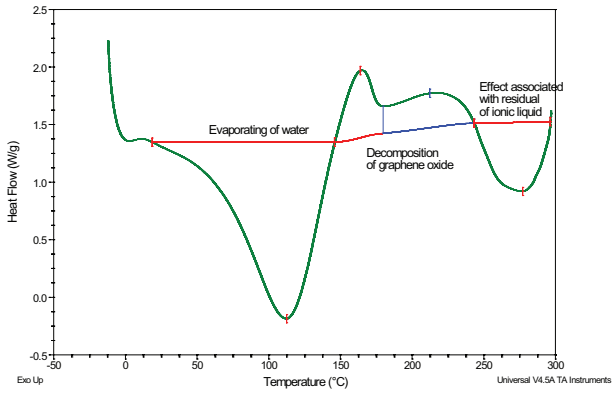

Fig. 7. Transitions occurred in material of membranes during the heating revealed on DSC curve.

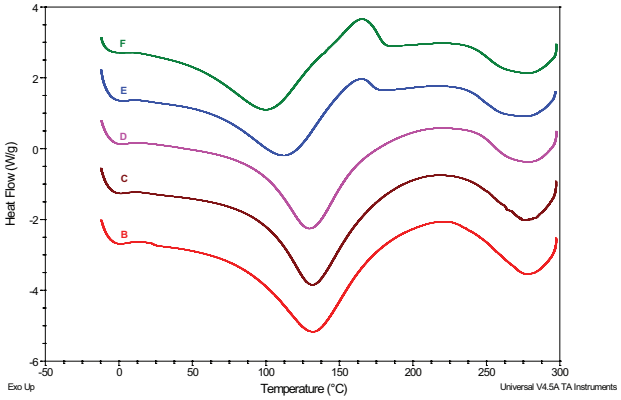

Fig. 8. DSC curves of composite GO/CEL membranes. Curves were registered at the heating mode with the rate of 20°/min in nitrogen atmosphere (flow 40 mL/min).

Table 2
Values of characteristic temperatures and enthalpies of: water evaporation and graphene oxide thermal decomposition evaluated on the basis of DSC curves (Fig. 8) for GO/CEL membranes with the different content of graphene oxide modifier

No	Membrane	GO content %	Temperature of water evaporation $T_{w\,ev}$/°C	Enthalpy of water evaporation $\Delta H_{w\,ev}$/°C	Temperature of GO decomposition $T_{GO\,d}$/°C	Enthalpy of GO decomposition $\Delta H_{GO\,d}$/J g^{-1}
1	A	0.1	124.0	209.2	215.5	36.1
2	B	0.2	132.0	259.0	219.6	55.8
3	C	1.0	130.9	259.3	218.5	56.0
4	D	2.0	129.0	261.9	218.5	56.9
5	E	10.0	112.5	238.3	164.9/217.5	40.9/47.6
6	F	20.0	100.1	238.1	164.9 219.4	61.4/39.8

than 165°C and the enthalpy rising significantly from 40.9 to 61.4 J/g for a GO content of threshold of 20%.

The analysis of the presented calorimetric study results and the previous reference to presented WAXS diffraction study results (Fig. 6) allowed to conclude that in the case of relatively high content of graphite oxide, the excess modifier is separated and a separate GO phase appears in the composite membrane structure. The sizes of GO precipitates (grains) are large and clearly visible in SEM images (Fig. 3-1). In case of membrane E, these are single scales embedded in a single GO/CEL matrix. In the case of membrane F (as a characteristic structure) almost all its volume is filled with flakes. The second GO phase, whose presence was confirmed throughout the entire series of composite membranes, is dispersed in the cellulose matrix well enough to not be visible in SEM images. This phase decomposes at temperatures significantly higher (by over 50°C), which is reflected directly in the DSC curves. This fact is confirmed by previously mentioned literature [48] and the results of FTIR studies presented in this paper, whose analysis showed the presence of hydrogen bonds between oxygen atoms of effectively exfoliated graphene GO surfaces, and hydrogen atoms of cellulose hydroxyl groups.

At this point, it is worth to emphasize the pioneering nature of the DSC results of GO/CEL membranes presented above. Calorimetric studies proved to be particularly useful in correspondence to SEM, WAXS and FTIR techniques. Previous literature reports on thermal studies of this type of materials were practically limited to the use of TGA.

3.2. Transport properties of membranes

An important parameter determining the transport properties of membranes is the specific permeate flux (Fig. 9). As a result of the experiment, cellulose membranes (membrane "0") and cellulose composite membranes (membranes A–F) were obtained which, depending on the qualitative composition, differed in their transport properties. The lowest values of volumetric permeate flux were recorded for the membrane "0," and for the subsequent pressures of 0.1; 0.15 and 0.2 MPa, were respectively: 2.93 ± 0.02; 3.76 ± 0.07 and 4.36 ± 0.03 L/m² × h. Slow but slight increase in the permeate flux, which is observed with the increase of working pressure, may indicate a compact structure of membrane "0". It can therefore be assumed that membrane "0" is composed of closed pores, which is confirmed by SEM images Fig. 3("0"-1).

The transport properties of the composite membranes A, B and C are similar. The permeate flux for these membranes increases slowly with the increase in working pressure and for 0.2 MPa it is: 4.58 ± 0.32 (membrane A); 5.26 ± 0.10 (membrane B); 5.43 ± 0.07 (membrane C) L/m² × h, respectively. The results show that the addition of 0.1% w/w; 0.2% w/w; 1.0% w/w of GO to the cellulose only slightly improves the transport properties of the obtained GO/CEL membranes. In the case of membranes A and B, it can be assumed that the structures observed in SEM images contain mainly closed pores. However, in the case of the C membrane, low values of the permeate water flux may be a result of the formation of hydrogen bonds between GO molecules and cellulose chains (Fig. 1), which result in hydrophobic of membrane described in our earlier publication [57]. This can be confirmed by the low thickness of the C membrane observed in SEM images (Fig. 3(C-1)).

Increase in the distilled water flow through cellulose composite membranes is observed for GO addition at a concentration of 2% w/w; 10% w/w; 20% w/w. The permeate volumetric flux values for the working pressure of 0.2 MPa are: 10.24 ± 0.22 (membrane D); 21.71 ± 0.68 (membrane E); 40.20 ± 2.33 (membrane F) L/m² × h, respectively. The results shows that the addition of GO to cellulose in amounts of 2% w/w; 10% w/w; 20% w/w improves the transport properties of the obtained GO/CEL membranes 2, 5, 10 times in comparison with the membrane "0". Thus, it can be assumed that membranes D, E, F due to the large amount of GO, have a layered structure (Figs. 3(D-1), (E-1) and (F-1)) which facilitates the transport of water despite the high thickness of these composite membranes.

Studies on the transport properties of membranes based on pure CEL and GO/CEL composites indicated the possibility of using the obtained membranes for the separation of metals. Pure cellulose membrane ("0"), and membranes D, E and F, which were characterized by definitely high permeate flux values, were selected for the separation properties investigations (Fig. 9). The investigations were carried out for each salt solution separately (individual ions and mixture of synthetic wastewater) and for each membrane separately (Fig. 10).

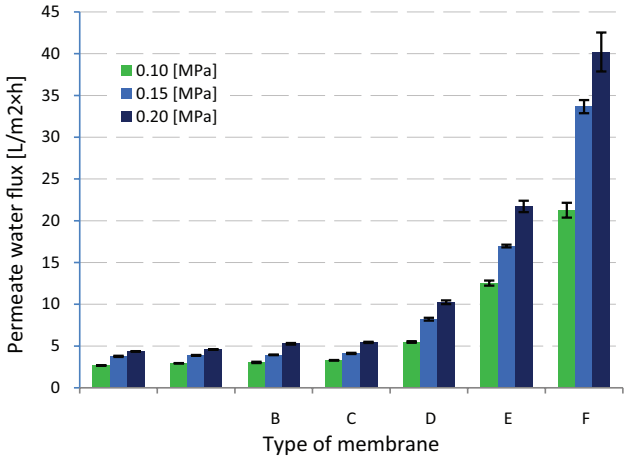

Fig. 9. Pure water permeability for pure cellulose membrane and GO/CEL composite membranes.

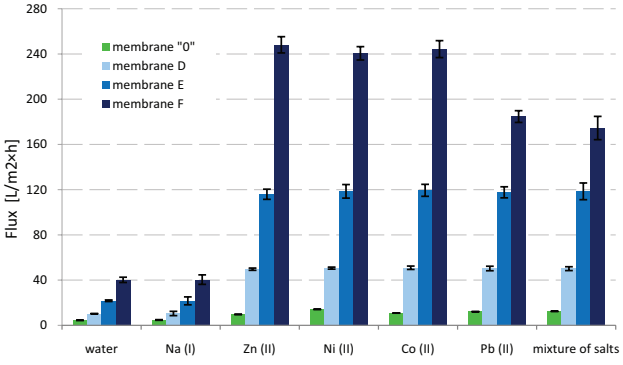

Fig. 10. Volumetric permeate flux for individual ions and synthetic wastewater mixture measured for pure cellulose membrane and selected GO/CEL composite membranes for working pressure of 0.2 MPa.

During the investigation of separation properties, a significant increase in the volumetric permeate flux was observed under the impact of the heavy metal ions flowing through the membranes (Fig. 10). For the membrane obtained from pure cellulose (membrane "0"), it was observed that the flow is 4.34 L/m² × h for distilled water, while the solutions of salts (bivalent ions) increased the flow through this membrane in the following order: zinc 9.6 L/m² × h, cobalt 10.80 L/m² × h, lead 12.08 L/m² × h and nickel 14.08 L/m² × h. In the case of synthetic wastewater mixtures, the permeate flux for the "0" membrane increases ~2.8 times relative to the flow of distilled water.

In the studies of transport properties of these membranes, it was observed that under the influence of the solution containing Zn(II), Ni(II) and Co(II) ions the permeate flux is increased five to six times and for successive ions is: 49.6; 50.6; 50.1 L/m² × h (membrane D); 115.9; 118.5; 119.4 L/m² × h (membrane E); 248.1; 240.6; 244.3 L/m² × h; (membrane F), respectively. While for the feed containing individual Pb(II) ions and a mixture of synthetic wastewater, it was observed that the permeate flux was 50.3; 50.1 L/m² × h (membrane D); 117.6; 118.5 L/m² × h (membrane E); 184.6; 174.5 L/m² × h (membrane F). During the investigation, it was observed that sodium ions do not affect the volumetric permeate flux at all.

3.3. Separation properties of membranes

As a result of the transport properties studies, it was observed that the membranes produced in the experiment can be used to remove bivalent heavy metal ions from aqueous solutions. All obtained membranes, both of pure cellulose and cellulose with addition, are characterized by high rejection coefficient (*R*) values. Membrane "0" (Fig. 11(a)) is characterized by a rejection coefficient which, for the subsequent ions, was: 100% (Co); 93% (Zn); ~69% (Pb); 40% (Ni); 1% (Na), respectively. On the other hand, the studies carried out on the synthetic waste water mixture (Fig. 11(b)) showed that the *R* coefficient for the pure cellulose membrane was: 100% (Co); ~87% (Zn); ~71% (Pb); ~79% (Ni), ~2% (Na), respectively. Comparing the results obtained, it was observed that in the mixture of synthetic wastewater, the preferential rejection of nickel ions on the membrane "0" and the increase in the degree of lead ion rejection with respect to zinc ions, for which the *R*-coefficient decreases, occurred.

All cellulose GO/CEL composite membranes studied in the experiment are characterized by higher rejection coefficient values than membrane "0" (Fig. 11). Thus, the nanoaddition of GO in the cellulose matrix increases the amount of heavy metal ions deposited on the membranes. By analysing the results obtained for membrane D, it can be observed that 2% w/w of GO addition results in the highest values of *R* coefficient, which is 100% (Co); 98%–100% (Zn); 97% – 99% (Ni); 69% – 71% (Pb), respectively. And the increase in the amount of GO addition to 10% or 20% does not improve the degree of ion rejection on membranes, but even slightly decreases it by 1%.

The explanation of the observed phenomenon may be too high concentration of GO in the composite, resulting in the formation of layers and cracks, which were observed in cross sections (Figs. 3(D-1), (E-1) and (F-1)). We do not know exactly how the cellulose and GO layers arrange in our

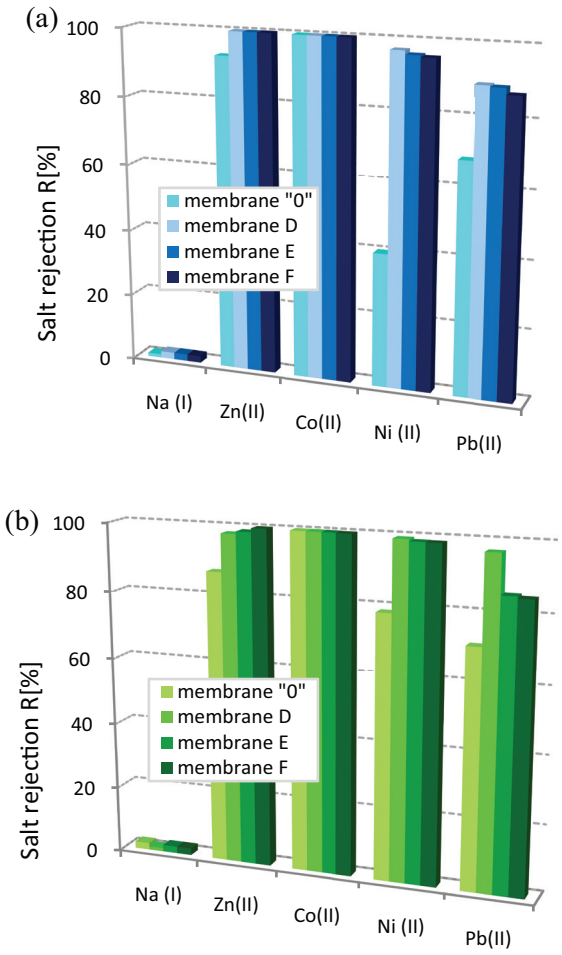

Fig. 11. Rejection coefficient on pure cellulose membrane and GO/CEL composite membranes of (a) single metals; (b) subsequent metals in synthetic wastewater.

composite. However, Chen et al. [58] show that the arrangement of electronegative and electropositive components of the composite is responsible for the separation properties of the membranes and the order in which heavy metals are removed from the solutions.

The results of the study show that the membranes obtained in the experiment are characterized by very high rejection coefficient values in relation to divalent metal ions of cobalt, zinc, nickel and lead. For Co(II) ions, total rejection is observed on each studied membrane, both for the solution containing single ions and for the synthetic wastewater mixture. In the case of other ions, on the other hand, the degree of rejection (*R*) of divalent ions is in the range of 85%–99%. Low rejection coefficient for sodium ions (1%–2%) indicates that we have obtained an UF membrane.

The observed changes may be the result of interactions between functional groups of cellulose chains and metal ions. The cellulose membrane is charged negatively and the charge is derived from hydroxyl groups (primary and secondary), which, according to Lewis theory, are hard bases. Co^{2+}, Ni^{2+}, Zn^{2+}, Pb^{2+} ions, on the other hand, are indirect acids. Thus, forming chemical (ionic and hydrogen) bonds between metal ions, cellulose chains is possible. The resulting combination

Table 3
Comparison of properties of membranes used to remove heavy metals

Membrane	J_v (L/m² × h)	Ion	Testing condition	Rejection (%)	References
HPEI-modified GO & EDA	5.01	$Pb(NO_3)_2$	1 mg/L, 0.1 MPa	95.7 ± 0.7	[59]
		$NiCl_2$	1 mg/L, 0.1 MPa	96.0 ± 3.8	
		$ZnCl_2$	1 mg/L, 0.1 MPa	97.4 ± 2.0	
Membrane D	10.24	$Pb(NO_3)_2$	60 mg/L, 0.2 MPa	89.3 ± 2.9	This work
		$Ni(NO_3)_2$	6 mg/L, 0.2 MPa	97.3 ± 3.0	
		$ZnCl_2$	6 mg/L, 0.2 MPa	100	
Membrane E	21.71	$Pb(NO_3)_2$	60 mg/L, 0.2 MPa	88.8 ± 4.1	This work
		$Ni(NO_3)_2$	6 mg/L, 0.2 MPa	96.2 ± 2.4	
		$ZnCl_2$	6 mg/L, 0.2 MPa	100	
Membrane F	40.20	$Pb(NO_3)_2$	60 mg/L, 0.2 MPa	87.0 ± 3.9	This work
		$Ni(NO_3)_2$	6 mg/L, 0.2 MPa	95.7 ± 2.5	
		$ZnCl_2$	6 mg/L, 0.2 MPa	100	

rejects heavy metal ions on the membrane but does not cause fouling. The increase in the permeate flow, on the other hand, may result from the formation of channels through which small particles of water flow freely.

Comparison of the results we obtained with literature data is difficult because there are no studies on the use of this type of membranes for heavy metal separation. The literature is broadly describing studies in which the membrane separation layer is GO in pure or modified form. In Table 3, an attempt was made to compare the results of the studies discussed above with those of Zhang et al. [59]. In the cited work, GO modified with ethylenediamine (EDA) and hyperbranched polyethyleneimine (HPEI), constituted a separation (skin) layer of polycarbonate membrane. Comparing the membranes from the study by Zhang et al. [59] to the GO/CEL composite membranes, similar rejection coefficient values can be observed for solutions containing nickel and zinc ions, although, in our experiment, six times higher concentrations were used. Comparison of the lead ions rejection factor leads to slightly lower values for membranes D, E, F, while the Pb^{2+} concentration used is 60 times higher than that the one reported by Zhang et al. [59]. It has also been observed that GO/CEL composite membranes show 2, 4 and 8 times greater permeate flux values than for HPEI membrane modified with GO & EDA.

4. Conclusions

Introduction of GO into the cellulose matrix influenced the process of membrane formation and, consequently, physicochemical, transport and separation properties of GO/CEL composite membranes. Structural studies (WAXS, FTIR, DSC) have shown the formation of hydrogen bonds between GO and CEL. In addition, they have shown that the incorporation of a small GO additive into the cellulose membranes results in a homogeneous composite in which the individual components are connected by hydrogen bonds. The use of SEM, WAXS and DSC allowed to state that in the case of a relatively high GO content, the excess admixture separates and an isolated GO phase occurs in the GO/CEL composite membrane structure, and it is responsible for very good transport and separation membrane properties. Composite membranes containing 2%, 10%, 20% GO have a very good rejection of heavy metal ions. Due to the bactericidal GO admixture, CEL/GO composite membranes can also find a potential application for water disinfection [60].

Acknowledgement

The authors would like to thank M. Sieradzka, M.Sc., for the synthesis of GO.

References

[1] B. Song, G. Zeng, J. Gong, J. Liang, P. Xu, Z. Liu, Y. Zhang, C. Zhang, M. Cheng, Y. Liu, S. Ye, H. Yi, X. Ren, Evaluation methods for assessing effectiveness of in situ remediation of soil and sediment contaminated with organic pollutants and heavy metals, Environ. Int., 105 (2017) 43–55.
[2] K. Vijayalakshmi, B.M. Devi, S. Latha, T. Gomathi, P.N. Sudha, J. Venkatesan, S. Anil, Batch adsorption and desorption studies on the removal of lead (II) from aqueous solution using nanochitosan/sodium alginate/microcrystalline cellulose beads, Int. J. Biol. Macromol., 104 (2016) 1483–1494.
[3] D.W. O'Connell, C. Birkinshaw, T.F. O'Dwyer, Heavy metal adsorbents prepared from the modification of cellulose: a review, Bioresour. Technol., 99 (2008) 6709–6724.
[4] L. Li, J. Dong, T.M. Nenoff, Transport of water and alkali metal ions through MFI zeolite membranes during reverse osmosis, Sep. Purif. Technol., 53 (2007) 42–48.
[5] F. Fu, Q. Wang, Removal of heavy metal ions from wastewaters: a review, J. Environ. Manage., 92 (2011) 407–418.
[6] S.K. Ramamoorthy, M. Skrifvars, A. Persson, A review of natural fibers used in biocomposites: plant, animal and regenerated cellulose fibers, Polym. Rev., 55 (2015) 107–162.
[7] W. Yang, B. Fang, Y.Y. Tang, Fast and accurate vanishing point detection and its application in inverse perspective mapping of structured road, IEEE Trans. Syst. Man Cybern. Syst., (2016) 1–12.
[8] F. Wendler, F. Meister, D. Wawro, E. Wesolowska, D. Ciechańska, B. Saake, J. Puls, N. le Moigne, P. Navard, Polysaccharide blend fibres formed from NaOH, N-methylmorpholine-N-oxide and 1-Ethyl-3-methylimidazolium acetate, Fibres Text. East. Eur., 79 (2010) 21–30.

[9] A. Pinkert, K.N. Marsh, S. Pang, M.P. Staiger, Ionic liquids and their interaction with cellulose, Chem. Rev., 109 (2009) 6712–6728.
[10] B. Lindman, G. Karlström, L. Stigsson, On the mechanism of dissolution of cellulose, J. Mol. Liq., 156 (2010) 76–81.
[11] H.P. Fink, P. Weigel, H.J. Purz, J. Ganster, Structure formation of regenerated cellulose materials from NMMO-solutions, Prog. Polym. Sci., 26 (2001) 1473–1524.
[12] S. Wang, A. Lu, L. Zhang, Recent advances in regenerated cellulose materials, Prog. Polym. Sci., 53 (2016) 169–206.
[13] R.P. Swatloski, J.D. Holbrey, R.D. Rogers, Ionic liquids are not always green: hydrolysis of 1-butyl-3-methylimidazolium hexafluorophosphate, Green Chem., 5 (2003) 361.
[14] N. Gathergood, M.T. Garcia, P.J. Scammells, Biodegradable ionic liquids: Part I. Concept, preliminary targets and evaluation, Green Chem., 6 (2004) 166.
[15] N.P. Novoselov, E.S. Sashina, O.G. Kuz'mina, S.V. Troshenkova, Ionic liquids and their use for the dissolution of natural polymers, Russ. J. Gen. Chem., 77 (2007) 1395–1405.
[16] S. Zhu, Y. Wu, Q. Chen, Z. Yu, C. Wang, S. Jin, Y. Ding, G. Wu, Dissolution of cellulose with ionic liquids and its application: a mini-review, Green Chem., 8 (2006) 325–327.
[17] C.R. Rambo, D.O.S. Recouvreux, C.A. Carminatti, A.K. Pitlovanciv, R.V. Antônio, L.M. Porto, Template assisted synthesis of porous nanofibrous cellulose membranes for tissue engineering, Mater. Sci. Eng. C, 28 (2008) 549–554.
[18] Y.N. Kuo, J. Hong, A new method for cellulose membrane fabrication and the determination of its characteristics, J. Colloid Interface Sci., 285 (2005) 232–238.
[19] W. Xiao, W. Yin, S. Xia, P. Ma, The study of factors affecting the enzymatic hydrolysis of cellulose after ionic liquid pretreatment, Carbohydr. Polym., 87 (2012) 2019–2023.
[20] H. Zhao, C.L. Jones, G.A. Baker, S. Xia, O. Olubajo, V.N. Person, Regenerating cellulose from ionic liquids for an accelerated enzymatic hydrolysis, J. Biotechnol., 139 (2009) 47–54.
[21] C. Ślusarczyk, B. Fryczkowska, M. Sieradzka, J. Janicki, Small-angle X-ray scattering studies of pore structure in cellulose membranes, Acta Phys. Pol. A, 129 (2016) 229–232.
[22] Å. Östlund, A. Idström, C. Olsson, P.T. Larsson, L. Nordstierna, Modification of crystallinity and pore size distribution in coagulated cellulose films, Cellulose, 20 (2013) 1657–1667.
[23] J. Guerrero-Contreras, F. Caballero-Briones, Graphene oxide powders with different oxidation degree, prepared by synthesis variations of the Hummers method, Mater. Chem. Phys., 153 (2015) 209–220.
[24] T. Ghosh, C. Biswas, J. Oh, G. Arabale, T. Hwang, N.D. Luong, M. Jin, Y.H. Lee, J. Do Nam, Solution-processed graphite membrane from reassembled graphene oxide, Chem. Mater., 24 (2012) 594–599.
[25] K.Y. Yoon, S.J. An, Y. Chen, J.H. Lee, S.L. Bryant, R.S. Ruoff, C. Huh, K.P. Johnston, Graphene oxide nanoplatelet dispersions in concentrated NaCl and stabilization of oil/water emulsions, J. Colloid Interface Sci., 403 (2013) 1–6.
[26] J. Texter, Graphene dispersions, Curr. Opin. Colloid Interface Sci., 19 (2014) 163–174.
[27] B. Konkena, S. Vasudevan, Understanding aqueous dispersibility of graphene oxide and reduced graphene oxide through p K a measurements, J. Phys. Chem. Lett., 3 (2012) 867–872.
[28] J.I. Parades, S. Villar-Rodil, A. Martínez-Alonso, J.M.D. Tascón, Graphene oxide dispersions in organic solvents, Langmuir, 24 (2008) 10560–10564.
[29] K. Goh, L. Setiawan, L. Wei, W. Jiang, R. Wang, Y. Chen, Fabrication of novel functionalized multi-walled carbon nanotube immobilized hollow fiber membranes for enhanced performance in forward osmosis process, J. Membr. Sci., 446 (2013) 244–254.
[30] R. Das, M.E. Ali, S.B.A. Hamid, S. Ramakrishna, Z.Z. Chowdhury, Carbon nanotube membranes for water purification: a bright future in water desalination, Desalination, 336 (2014) 97–109.
[31] B.J. Hinds, N. Chopra, T. Rantell, R. Andrews, V. Gavalas, L.G. Bachas, Aligned multiwalled carbon nanotube membranes., Science, 303 (2004) 62–65.
[32] E. Celik, H. Park, H. Choi, H. Choi, Carbon nanotube blended polyethersulfone membranes for fouling control in water treatment, Water Res., 45 (2011) 274–282.
[33] K.A. Mahmoud, B. Mansoor, A. Mansour, M. Khraisheh, Functional graphene nanosheets: the next generation membranes for water desalination, Desalination, 356 (2015) 208–225.
[34] Y. Han, Z. Xu, C. Gao, Ultrathin graphene nanofiltration membrane for water purification, Adv. Funct. Mater., 23 (2013) 3693–3700.
[35] R.K. Joshi, S. Alwarappan, M. Yoshimura, V. Sahajwalla, Y. Nishina, Graphene oxide: the new membrane material, Appl. Mater. Today, 1 (2015) 1–12.
[36] L. He, L.F. Dumée, C. Feng, L. Velleman, R. Reis, F. She, W. Gao, L. Kong, Promoted water transport across graphene oxide–poly(amide) thin film composite membranes and their antibacterial activity, Desalination, 365 (2015) 126–135.
[37] M.J. Park, S. Phuntsho, T. He, G.M. Nisola, L.D. Tijing, X.-M. Li, G. Chen, W.-J. Chung, H.K. Shon, Graphene oxide incorporated polysulfone substrate for the fabrication of flat-sheet thin-film composite forward osmosis membranes, J. Membr. Sci., 493 (2015) 496–507.
[38] S. Xia, M. Ni, T. Zhu, Y. Zhao, N. Li, Ultrathin graphene oxide nanosheet membranes with various d-spacing assembled using the pressure-assisted filtration method for removing natural organic matter, Desalination, 371 (2015) 78–87.
[39] A.F. Faria, C. Liu, M. Xie, F. Perreault, L.D. Nghiem, J. Ma, M. Elimelech, Thin-film composite forward osmosis membranes functionalized with graphene oxide–silver nanocomposites for biofouling control, J. Membr. Sci., 525 (2017) 146–156.
[40] P.S. Goh, A.F. Ismail, Graphene-based nanomaterial: the state-of-the-art material for cutting edge desalination technology, Desalination, 356 (2015) 115–128.
[41] R.R. Nair, H.A. Wu, P.N. Jayaram, I.V. Grigorieva, A.K. Geim, Unimpeded permeation of water through helium-leak-tight graphene-based membranes, Science, 335 (2012) 442–444.
[42] M. Bhadra, S. Roy, S. Mitra, Desalination across a graphene oxide membrane via direct contact membrane distillation, Desalination, 378 (2016) 37–43.
[43] T. Hwang, J.-S. Oh, W. Yim, J.-D. Nam, C. Bae, H.-I. Kim, K.J. Kim, Ultrafiltration using graphene oxide surface-embedded polysulfone membranes, Sep. Purif. Technol., 166 (2016) 41–47.
[44] G. Liu, H. Ye, A. Li, C. Zhu, H. Jiang, Y. Liu, K. Han, Y. Zhou, Graphene oxide for high-efficiency separation membranes: role of electrostatic interactions, Carbon N. Y., 110 (2016) 56–61.
[45] A. Kafy, A. Akther, M.I.R. Shishir, H.C. Kim, Y. Yun, J. Kim, Cellulose nanocrystal/graphene oxide composite film as humidity sensor, Sens. Actuators, A, 247 (2016) 221–226.
[46] C.J. Kim, W. Khan, D.H. Kim, K.S. Cho, S.Y. Park, Graphene oxide/cellulose composite using NMMO monohydrate, Carbohydr. Polym., 86 (2011) 903–909.
[47] C. Wan, J. Li, Graphene oxide/cellulose aerogels nanocomposite: preparation, pyrolysis, and application for electromagnetic interference shielding, Carbohydr. Polym., 150 (2016) 172–179.
[48] X. Zhang, H. Yu, H. Yang, Y. Wan, H. Hu, Z. Zhai, J. Qin, Graphene oxide caged in cellulose microbeads for removal of malachite green dye from aqueous solution, J. Colloid Interface Sci., 437 (2015) 277–282.
[49] W. Zhu, W. Li, Y. He, T. Duan, In-situ biopreparation of biocompatible bacterial cellulose/graphene oxide composites pellets, Appl. Surf. Sci, 338 (2015) 22–26.
[50] X.N. Yang, D.D. Xue, J.Y. Li, M. Liu, S.R. Jia, L.Q. Chu, F. Wahid, Y.M. Zhang, C. Zhong, Improvement of antimicrobial activity of graphene oxide/bacterial cellulose nanocomposites through the electrostatic modification, Carbohydr. Polym., 136 (2016) 1152–1160.
[51] X. Rui-Hong, R. Peng-Gang, H. Jian, R. Fang, R. Lian-Zhen, S. Zhen-Feng, Preparation and properties of graphene oxide-regenerated cellulose/polyvinyl alcohol hydrogel with pH-sensitive behavior, Carbohydr. Polym., 138 (2016) 222–228.
[52] L. Tang, X. Li, D. Du, C. He, Fabrication of multilayer films from regenerated cellulose and graphene oxide through layer-by-layer assembly, Prog. Nat. Sci. Mater. Int., 22 (2012) 341–346.

[53] W.S. Hummers, R.E. Offeman, Preparation of Graphitic Oxide, J. Am. Chem. Soc., 80 (1958) 1339–1339.
[54] K.M. Gupta, Z. Hu, J. Jiang, Mechanistic understanding of interactions between cellulose and ionic liquids: a molecular simulation study, Polymer (Guildf), 52 (2011) 5904–5911.
[55] Y. Cao, J. Wu, J. Zhang, H. Li, Y. Zhang, J. He, Room temperature ionic liquids (RTILs): a new and versatile platform for cellulose processing and derivatization, Chem. Eng. J. 147 (2009) 13–21.
[56] B. Fryczkowska, M. Sieradzka, E. Sarna, R. Fryczkowski, J. Janicki, Influence of a graphene oxide additive and the conditions of membrane formation on the morphology and separative properties of poly(vinylidene fluoride) membranes, J. Appl. Polym. Sci., 132 (2015) 42789.
[57] B. Fryczkowska, K. Wiechniak, Preparation and properties of cellulose membranes with graphene oxide addition, Pol. J. Chem. Technol., 19 (2017) 41–49.
[58] Y. Chen, F. Liu, Y. Wang, H. Lin, L. Han, A tight nanofiltration membrane with multi-charged nanofilms for high rejection to concentrated salts, J. Membr. Sci., 537 (2017) 407–415.
[59] Y. Zhang, S. Zhang, T.-S. Chung, Nanometric graphene oxide framework membranes with enhanced heavy metal removal via nanofiltration, Environ. Sci. Technol., 49 (2015) 10235–10242.
[60] B. Song, C. Zhang, G. Zeng, J. Gong, Y. Chang, Y. Jiang, Antibacterial properties and mechanism of graphene oxide-silver nanocomposites as bactericidal agents for water disinfection, Arch. Biochem. Biophys., 604 (2016) 167–176.